Final Progress Report: Due April 1st, 2020

"A Novel Supramacromolecular Approach to Non-toxic Combination Anti-cancer Therapeutics"

Jonathan Barnes, PhD
Department of Chemistry
Washington University in St. Louis

General Summary

Combination therapies – or drug 'cocktails' – are often employed to combat diseases such as cancer, and although effective, the drug combinations can be incredibly invasive due to off-target toxicity issues. Nano-based drug delivery systems can be advantageous in this regard since the toxic drugs can be shielded inside the nanomaterial and these non-specific issues can be reduced. However, it is still a major challenge to find a one-size-fits-all drug delivery vehicle that can be loaded and unloaded with any combination of small-molecule drugs without having to change the chemistry significantly each time a new clinically relevant combination is needed. The research in the Barnes group employs functional polymers that possess selective drug binding sites that can encapsulate a wide range of anti-cancer drugs through specific interactions, as well as monomers that serve as imaging agents that will allow for *in vivo* tracking of the nanomaterial. These polymers maybe cross-linked to generate nanoparticles, resulting in a water-stable vehicle that is a non-toxic and versatile platform for delivering combinations of anti-cancer therapeutics.

During the second and final year of support from the Cancer Research Foundation (CRF), the Barnes group has been able to (i) complete the synthesis and polymerization of functional monomers bearing drug-binding sites, (ii) demonstrate the binding of several anti-cancer drugs inside the cavities of the macrocycles attached to the polymer, (iii) self-assemble the drug-loaded polymers into nanoparticles, and (iv) demonstrate cytocompatibility against healthy human cells, while also showing the ability to permeate cell membranes to aid in drug delivery. During the second year of support from CRF, we also developed an entirely new type of polymer that has a drug-binding core made of sugars and an overall star-like architecture, which we showed could deliver the anti-cancer drug doxorubicin to MCF-7 breast cancer cells, while preserving cytocompatibility with non-cancerous endothelial cells.

Background & Motivation

Many debilitating and aggressive diseases, such as cancer, HIV/AIDS, and multi-drug resistant (MDR) bacterial infections, for example, require combination therapies consisting of multiple small-molecule drugs working in concert.[1] These so-called drug 'cocktails' are capable of overcoming potential issues of drug resistance since the correct ratio of drugs can often result in a synergistic effect, where each drug has orthogonal targets and mechanisms of action. One example of a combination-based strategy is FOLFIRINOX – consisting of Folinic acid, Fluorouracil, Irinotecan, and Oxaliplatin – which is often used to treat metastatic pancreatic cancer.[2] Although it is an effective treatment capable of extending the median overall survival rate to 11.1 months (compared to only a few months with other single-drug-based systems), FOLFIRINOX is also incredibly toxic and may result in an increased rate of infection due to a drop in white blood cells, tiredness as a result of a lower red blood cell count, the formation of ulcers, hair loss, and so on.

Over the past several decades, the drug delivery community has worked to develop systems capable of delivering small-molecule drugs with improved pharmacokinetics and dramatically reduced toxicities,[3] however, it remains a major challenge to construct nano-based platforms that can support the precise loading of three or more drugs, and release them in a well-controlled and concerted manner without inducing off-target toxicity issues. Although there are many different types of drug delivery nanomaterials[4] that have been developed over the years (Fig. 1), most of them fall under two main categories in relation to how drugs are loaded and released. The first utilizes an encapsulation strategy, whether it be in the pores of mesoporous silica nanoparticles (MSNPs)[5] or trapped in the hydrophobic region of a polymer-based micelle,[6] for example. This non-specific approach can result in NPs that prematurely release their drug cargo in the blood stream (Fig. 2, left), an outcome which may result in off-target toxicity and lower doses reaching the site of diseased tissue. At the other end of the spectrum are nanomaterials where the drug is covalently bonded to the delivery substrate. For example, drug-conjugated polymers are one of the oldest strategies to deliver drugs with improved pharmacokinetics (i.e., longer half-lives in the blood) and solubilities,[7] however, this method relies on a chemical linker between the polymer and the small molecule drug. This type of chemical modification transforms the small-molecule free drug into a prodrug, which must then rely on an external actor inside the body – such as a change in pH or an enzyme – to cleave the prodrug, and ultimately release the intended free drug. If this strategy is applied for the purpose of delivering a single drug, then some percentage of drug will undoubtedly be unmasked and find its target. However, if the intent is to apply this strategy for

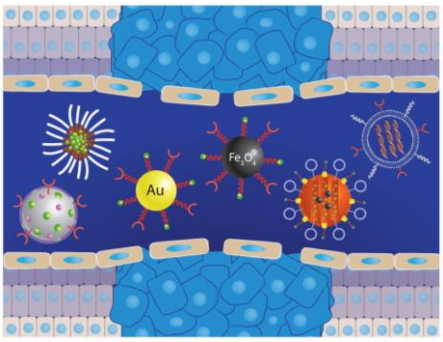

Figure 1. Different types of nano-based drug delivery systems that have been developed. Left to right: Liposome, polymeric micelle, gold nanoparticle (NP), iron oxide NP, mesoporous silica NP, and siRNA liposome complexes. (adapted from ref. 6)

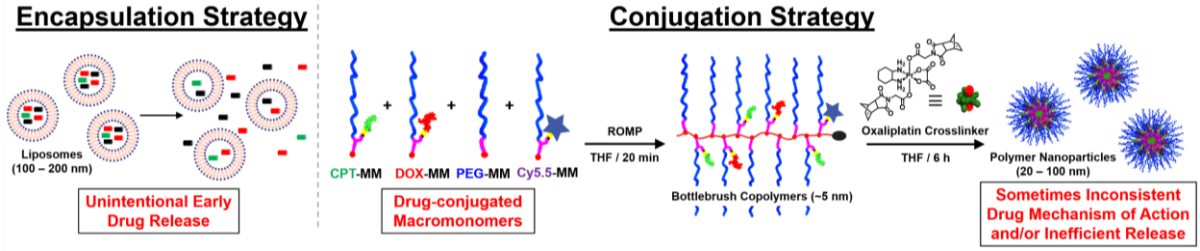

Figure 2. Comparison of a generic drug encapsulation strategy with liposomes versus a drug-conjugated strategy that I carried out as a postdoctoral fellow at MIT. Liposomes can result in early release, and conjugated drugs (i.e., prodrugs) can have different MOAs and exhibit inefficient release and nanoparticle degradation.

the delivery of a drug combination, then there may be some practical limitations. For example, I previously developed (Fig. 2, right) norbornene-based drug-conjugated macromonomers bearing doxorubicin (DOX) and camptothecin (CPT), which were converted into bottlebrush copolymers[8] via ring-opening metathesis polymerization (ROMP)[9,10] and subsequently crosslinked using a platinum prodrug (OxPt) adorned with two norbornene groups. This well-controlled synthesis afforded narrowly dispersed nanoparticles that displayed blood circulation half-lives between 4-6 hours after injection into BALB/c mice. Although the synthetic protocol consistently produced well-defined triply drug loaded nanoparticles, the reliance on esterases[11] to cleave the chemical linker between polymer substrate and the prodrug, and the lack of a clear degradative pathway to break down the NP, meant that the three drugs were not guaranteed to be released simultaneously and that uncleared residual nanomaterial could remain. Moreover, if a different combination of drugs is required to treat a different type of cancer, then new drug-conjugated macromonomers must be synthesized and the linkers tested for proper release under physiological conditions. These extra synthetic steps and screenings require more materials and time to investigate efficacy for each disease.

Description of Research Progress by PI

Instead of utilizing non-specific encapsulation or covalently tagging polymers with prodrugs, we employed macrocyclic chemistry[12] to program specific drug-binding receptors into a polymer-based nanomaterial. Specifically, my laboratory has synthesized the two norbornene-functionalized macrocyclic monomers shown in Fig. 3, where one is based on β-cyclodextrin[13] (**Nb-CD**; Fig. 3A) – which can bind a wide range of hydrophobic drugs (including both antibiotic and anticancer drugs; *vide infra*) – and the other consists of a thiacalix[4]arene (**Nb-TCA**; Fig. 3B), which is a smaller thioether-based macrocycle capable of binding silver ions (Ag^+) with high affinity.[14] This latter capability is very important as Collins and co-workers demonstrated[15] several years ago how sub-inhibitory levels of Ag^+ could potentiate antibiotics that were no

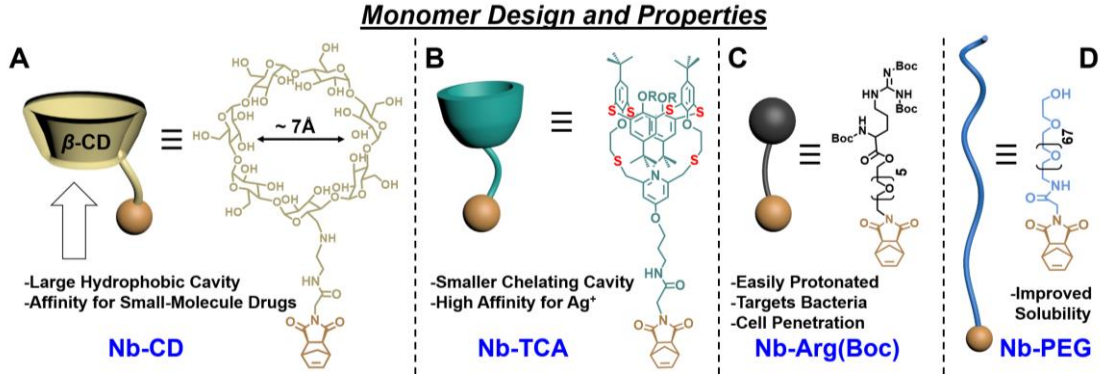

Figure 3. Chemical structures (and cartoon representations) for the four proposed functional monomers.

longer effective against drug-resistant bacteria. This is an important feature, as it allows us to use the polymer platform for both antimicrobial and anticancer applications. Additionally, we synthesized two more functional monomers, **Nb-Arg** and **Nb-PEG** (Fig. 3C-D, resp.). The former can be deprotected and a positively charged guanidinium group generated to aid with electrostatically targeting negatively charged outer membranes of bacteria, as well as serving as a cell penetrating peptide mimic,[16] whereas the latter PEG_{3000}-based monomer enhances the water solubility of any resultant copolymers. As a proof-of-concept, we carried out a series of ^1H NMR titrations investigating the binding affinity between **Nb-CD** and a wide range of antibiotic and anticancer drugs in H_2O (Fig. 4; 10^2–10^5 M^{-1}). The preliminary results indicate that **Nb-CD** is a suitable host to bind several different types of drugs and may be used in treating both bacterial infections, as well as cancer. Additionally, we carried out a similar titration for **Nb-TCA**, by adding a concentrated $AgNO_3$ solution in H_2O in increments to a THF solution containing the

host monomer. The binding under these conditions was quite high (THF:10^5 M^{-1}) and only somewhat lower in H_2O (10^4 M^{-1}).

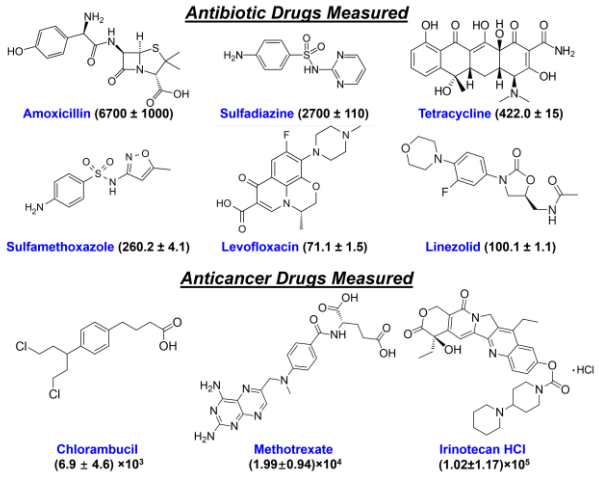

Figure 4. Library of antibiotics and anticancer drugs and their respective binding affinities (K_a) with **Nb-CD**.

With these functional monomers in hand, we next assessed the ability to polymerize each using standard ROMP chemistry and a Grubbs 3rd generation catalyst.[17] After much screening and optimization of the conditions to generate the homopolymers of each monomer, we were able to successfully generate the tetrablock copolymer shown in Fig. 5A (upper right). The theoretical molecular weight of the final water-soluble tetrablock copolymer **poly(Arg(Boc)-*b*-PEG-*b*-TCA-*b*-(Me-CD))** is around 80 kDa, where the molecular weight increased with each addition of functional monomer (Fig. 5B, see GPC data). Thus, these monomers still polymerize in a living manner,[18] reacting with the terminal ruthenium-carbene.[19,20] Next, the tetrablock copolymer was deprotected using trifluoroacetic acid (TFA), dialyzed against H_2O several times, and loaded with μM concentrations of Ag^+ (as $AgNO_3$) and amoxicillin. After letting the sample equilibrate for a few hours, the **Tetra-Ad** crosslinker (XL) was added in DMSO to the aqueous solution containing the copolymer/drug mixture. Within the time it took to load the sample into a cuvette and measure its hydrodynamic diameter via dynamic light scattering (DLS), the nanoparticles (~200 nm) had already formed as the XL's adamantane groups occupied 20% of the theoretical number of CD sites in the tetrablock copolymer. The same experiment was carried out again, except with 30% of the CD sites theoretically occupied, the resultant nanoparticles were found (by scanning tunneling electron microscopy, STEM, Fig. 5B) to possess a diameter that was nearly identical to the DLS values obtained in solution.

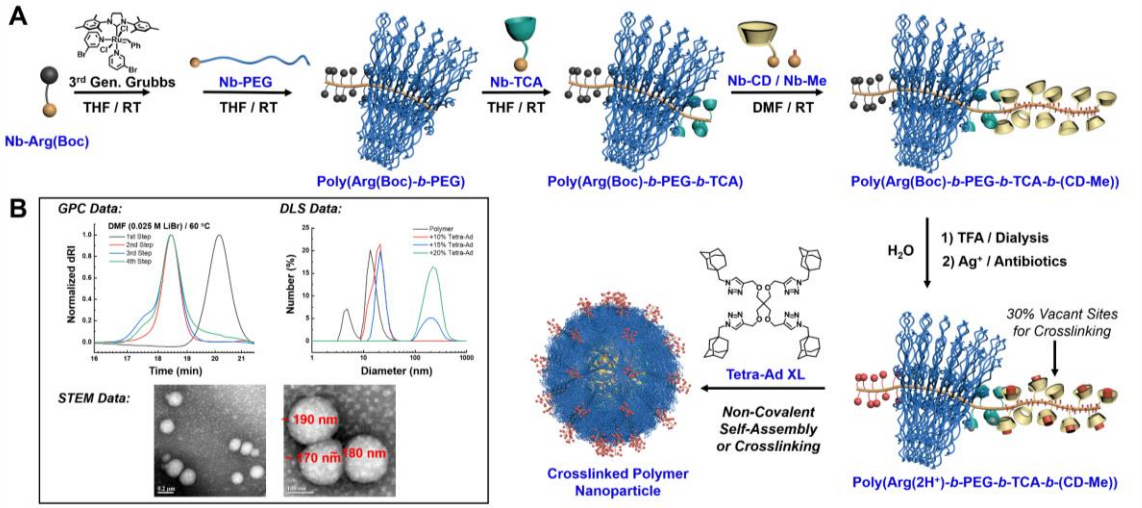

Figure 5. (**A**) Block copolymerization of each functional monomer into a tetrablock copolymer (**Poly(Arg(Boc)$_5$-*b*-PEG$_{20}$-*b*-TCA$_5$-*b*-(CD$_{30}$-Me$_{90}$))** ($M_{n,theor.}$ ~ 80 kDa). After deprotection of the Boc groups and dialysis against H_2O, the functional copolymer was loaded with μM quantities of Ag^+ and antibiotics, stirred for ~2 h, and **Tetra-Ad** crosslinker (XL) was added to form nanoparticles. (**B**) Normalized GPC traces show conversion of each monomer into polymer, and DLS and STEM data confirm nanoparticle formation upon addition of XL up to 20 and 30% occupancy, respectively.

a) Antibacterial Application of Polymeric Nanoparticles:

The toxicity of the Boc-deprotected nanoparticles (loaded with Ag^+ or Ag^+ & amoxicillin) against human umbilical vein endothelial cells (HUVEC) were evaluated (Fig. 6A) from 2.0–0.007 mg/ml of polymer nanoparticle (equating to 63.0–0.25 uM Ag^+ and 263.5–1.03 uM amoxicillin, respectively). After a 48 h incubation, the results indicate that the dual-loaded nanoparticles exhibit low toxicity near 1.0 mg/ml nanoparticle. To confirm that the free Ag^+ and amoxicillin can undergo slow release in the presence of bacteria (specifically non-resistant *S. aureus*, ATCC 11632), a 0.37 mg/ml nanoparticle solution was used in an agar-diffusion assay (Fig. 6B) and compared directly to the corresponding concentrations of free Ag^+ (11.9 uM) and free Ag^+ (11.9 uM) plus amoxicillin (50 uM). As expected, the combination of Ag^+ and amoxicillin resulted in the largest zone of growth inhibition, whereas the nanoparticle loaded with equivalent concentrations of Ag^+ and amoxicillin yielded a smaller zone after a 19 h incubation. We interpret these results to mean that the nanoparticle bound drugs underwent slower release from the core of the nanoparticle. It is also important to note that the unloaded polymer does not kill or inhibit bacteria in this assay and that sublethal concentrations of Ag^+ result in no inhibition of growth.

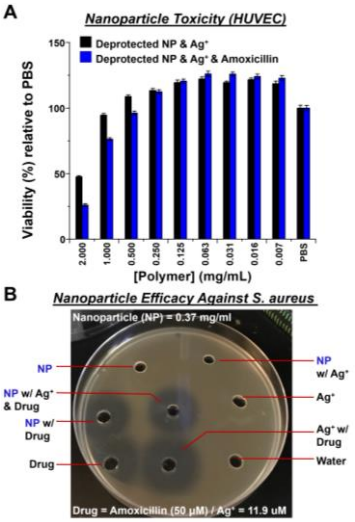

Figure 6. (**A**) Cytotoxicity results against HUVEC for deprotected nanoparticles (NP) loaded with only Ag^+ or with Ag^+ & amoxicillin. (**B**) Preliminary bacterial efficacy study against clinical isolate of *S. aureus* obtained from WUSTL School of Medicine. Both drug loaded and free drug cocktails at same concentrations were compared (see pic for conc.'s).

Future work towards antimicrobial applications involves the study of the nanoparticles loaded with different antibiotics and against different strains of drug-resistant bacteria. It is also important to study the nano-bio interface of the different bacteria cell lines, which we intend to investigate using membrane permeability assays and confocal microscopy. This work is currently underway in the Barnes group.

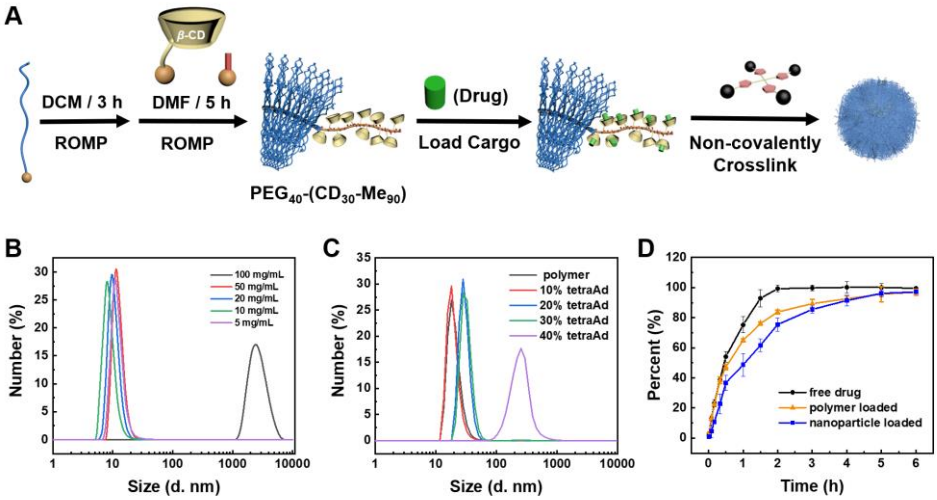

Figure 7. (**A**) Nanoparticles were synthesized again, except now with no TCA macrocycle, only CD macrocycles for binding anticancer drugs. (**B**) Dynamic light scattering (DLS) measurements were obtained for the non-crosslinked polymer at different concentrations. (**C**) The polymers were crosslinked at different concentrations of **Tetra-Ad** (in mol%), and the particle sizes measured by DLS. 40% **Tetra-Ad** yielded nanoparticles about 200 nm in diameter. (**D**) Drugs were released from just the dialysis bag (black trace), drug-loaded polymer (orangish yellow trace), and drug-loaded nanoparticles (blue trace) over 6 h.

b) Anticancer Application of Polymeric Nanoparticles:

Building off the developed nanoparticle platform, we next set out to test the approach for use in anticancer applications. The nanoparticles were synthesized (Fig. 7A) in the same way as described earlier, except without the TCA monomer because no Ag^+ was used for the anticancer study. Without the crosslinker (**Tetra-Ad**), the polymer did not produce aggregates or nanoparticles, even up to 100 mg/mL in H_2O (see DLS data in Fig. 7B). Upon addition of the crosslinker at different mol% values (Fig. 7C), the polymers could be crosslinked into nanoparticles capable of housing different drugs and drug combinations. As a proof-of-concept, the polymers were loaded with a coumarin dye that mimics the binding of small-molecule drugs in the cavity of the CD side chain. Release of the drug mimic from the nanoparticle was monitored over 6 h (Fig. 7D). The nanoparticle showed slower release than that from the dialysis bag alone (black trace), as well as the release of the drug from just the polymer alone (red trace). This is an important feature because it means that the drug can be stabilized inside the core of the nanoparticle for longer periods of time relative to existing in solution as the free drug.

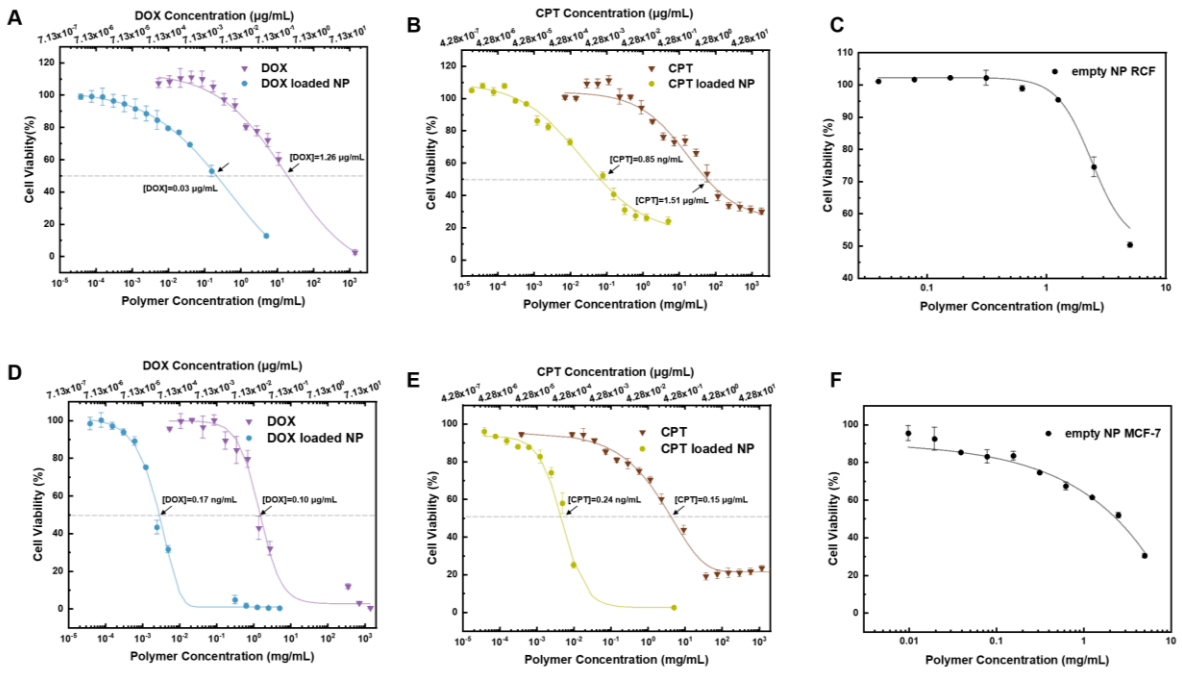

Figure 8. Cell *v*iability *s*tudies of RCF cells (**A**)–(**C**) and MCF-7 cells (**D**)–(**F**). (**A**) Cell viability of RCF cells against free DOX·HCl and nanoparticle-loaded DOX·HCl. (**B**) Cell viability of RCF cells against free CPT and nanoparticle-loaded CPT. (**C**) Cell viability of RCF cells against empty nanoparticle. (**D**) Cell viability of MCF-7 cells against free DOX·HCl and nanoparticle loaded DOX·HCl. (**E**) Cell viability of MCF-7 cells against free CPT and nanoparticle-loaded CPT. (**F**) Cell viability of MCF-7 cells against empty nanoparticle.

Once the nanoparticle self-assembly and drug release were confirmed, we next sought to test the cytotoxicity of the empty nanoparticles against healthy rat cardiac fibroblast (RCF) cells (Fig. 8C). This cell viability study revealed an IC_{50} of 4 mg/mL for the nanoparticle platform, demonstrating low toxicity. Then, we tested common anticancer drugs, doxorubicin (DOX) and camptothecin (CPT), in their free drug forms and encapsulated within the nanoparticles against RCF cells (Fig. 8A and 8B, respectively). Normally, DOX and CPT relatively soluble in aqueous growth media. As their free drug forms, this leads to IC_{50} values of 1.26 and 1.51 μg/mL for DOX and CPT, respectively. Once the drugs are encapsulated inside the nanoparticles, they become much more soluble in solution and their cellular uptake properties are dramatically improved. This claim is supported by the fact that the IC_{50} values for DOX-loaded nanoparticles and CPT-

loaded nanoparticles is 0.03 μg/mL and 0.85 ng/mL against RCF cells, respectively. The same viability studies were performed against MCF-7 breast cancer cells (Fig. 8D-F). For the empty nanoparticle, the IC_{50} value was 2 mg/mL (Fig. 8F), whereas the DOX- and CPT-loaded nanoparticles exhibited IC_{50} values (Fig. 8D-E) of 0.17 and 0.24 ng/mL, respectively. Again, we attribute the greater toxicity for DOX and CPT housed inside the nanoparticles to their enhanced solubility and cell uptake properties.

To confirm the nanoparticles are taken up by MCF-7 cells, we next treated the cells with a cyanine5.5 (Cy5.5) dye-loaded nanoparticle for 48 h. These cells were stained with Hoechst 33342 (nucleus) and CellMask orange (plasma membrane) (Note: this dye is supposed to dye the cell membrane as orange, but because we also have a red Cy5.5 dye, the detected signal was set as green to generate a high contrast image.) Fig. 9 shows each individual stain fluoresced separately and then merged (lower right image). It is clear from these images that the nanoparticles are readily taken up by the cells. Moving forward, we plan to quantify this uptake by doing the same experiment except using flow cytometry to discern how much of the nanoparticle dose makes it inside the cancer cells. Once we have this data in hand, the next phase of this research will involve characterizing the *in vivo* properties of the nanoparticles in mice in terms of their maximum tolerable dose, pharmacokinetics, biodistribution, and *in vivo* efficacy in a xenograft hind flank tumor model.

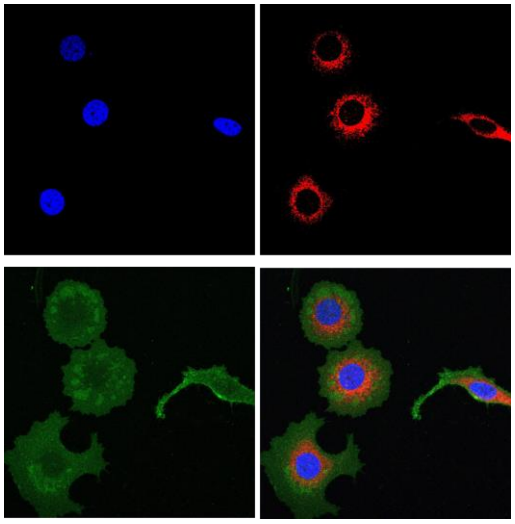

Figure 9. Confocal microscopy data showing cellular uptake of cyanine5.5 dye-conjugated nanoparticles into MCF-7 cancer cells. Blue stain in nucleus is Hoechst 33342, red color comes from Cy5.5 near IR fluorescent dye tethered to nanoparticle, and the green color is CellMask orange plasma membrane dye that was adjusted to give a green color for better contrast. The bottom right image is the merger of all three fluorescent dye images.

c) <u>Design and Synthesis of Well-defined γ-CD-based Star Polymers</u>

A new star polymer design and core-first/graft-from synthetic strategy described here is based on three main building blocks (Fig. 10a): *i)* a multifunctional initiator (**γ-CD-Nb$_8$**), *ii)* a norbornene-HEG monomer (**Nb-HEG**), and *iii)* a norbornene-PEG macromonomer (**Nb-PEG**). In the first step, **γ-CD-Nb$_8$** is activated by adding eight equiv. of Grubbs' 3rd generation catalyst in DMF at room temperature (Fig. 10b). Then, 8m·**Nb-HEG** is added to initiate polymerization of all eight arms, thus forming the homo-arm star polymer **CD-(HEG$_m$)$_8$**. Next, chain extension of the ω-functional arms is achieved by adding 8n·**Nb-PEG**, which produces the corresponding DBASC: **CD-(HEG$_m$-PEG$_n$)$_8$**.

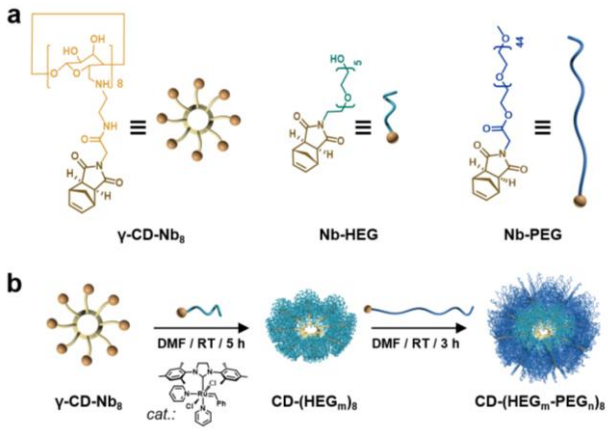

Figure 10. (a) Chemical structures and corresponding cartoon representations of **γ-CD-Nb$_8$**, **Nb-HEG**, and **Nb-PEG**. (b) Core-first/graft-from synthetic strategy for DBASCs (**CD-(HEG$_m$-PEG$_n$)$_8$**).

To enable the synthesis of the water-

soluble, eight-arm DBASCs, the primary alcohols of γ-CD were first converted to iodide leaving groups using triphenylphosphine, followed by nucleophilic substitution using ethylene diamine in dimethylformamide (DMF). The desired product (**γ-CD-$(NH_2)_8$**) was obtained after each step by dissolving the crude mixture in minimal solvent and precipitating in excess acetone (Me_2CO) three times, where the overall yield for the first two steps was 47%. To install the norbornene groups onto **γ-CD-$(NH_2)_8$**, an *N*-hydroxysuccinimide precursor (**Nb-NHS**) was synthesized by coupling a norbornene-glycine (**Nb-Gly**) derivative (see Supporting Information (SI) for its preparation) to NHS using *N*,*N*′-dicyclohexylcarbodiimide (DCC) in dichloromethane (CH_2Cl_2) at room temperature (70% yield). Then, one equiv. of **γ-CD-$(NH_2)_8$** and a slight excess (8.2 equiv.) of **Nb-NHS** were reacted in the presence of triethylamine (TEA) in DMF at 80 °C. The desired product (**γ-CD-Nb_8**) was obtained by re-dissolving the concentrated crude material in a minimal amount of DMF, followed by precipitation in excess Me_2CO to obtain pure product as a brown solid (60% yield). Product identity was determined using nuclear magnetic resonance (NMR) spectroscopy, as well as HPLC and gel permeation chromatography (GPC).

Dimensions and Physical Properties of the Well-defined DBASCs:

Characterization of the dimensions and physical properties of the well-defined DBASCs was performed using DLS, transmission electron microscopy (TEM), differential scanning calorimetry (DSC), thermal gravimetric analysis (TGA), and powder X-ray diffraction (PXRD). The morphology and size distribution of **CD-$(HEG_7$-$PEG_9)_8$** was first assessed by TEM (Fig. 11a). The deposition of the resultant star polymers on the TEM grid resulted in nanostructures that appeared crystalline and porous, adopting an almost "honeycomb" morphology. Analysis of the TEM data reveals a DBASC distribution (Fig. 11b) ranging from 5–30 nm in size, where the average size centred about 15 nm. In an aqueous solution, the three synthesized DBASCs possessed hydrodynamic diameters (D_h) between 10.0–11.0 nm at lower concentrations, where no aggregation was observed (Fig. 11c: **CD-$(HEG_7$-$PEG_9)_8$**. Although these D_h values are smaller than that measured using TEM, it is expected that aggregation on the TEM grid will result in larger sizes.

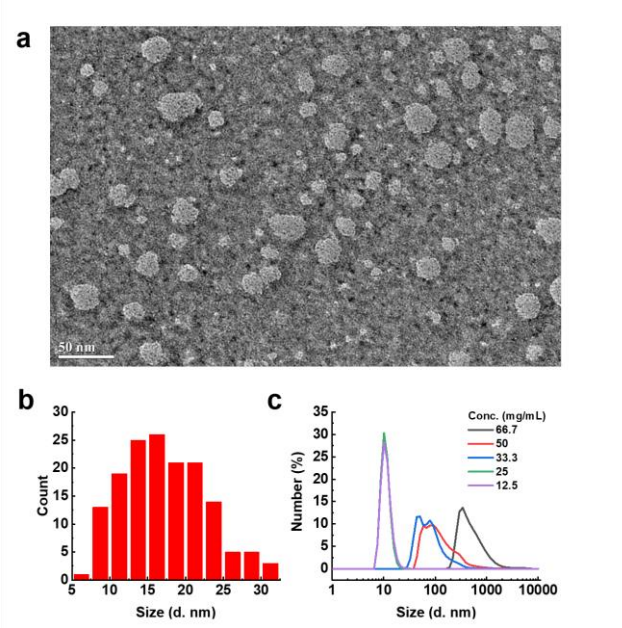

Figure 11. (a) TEM image showing **CD-$(HEG_7$-$PEG_9)_8$** (lighter colored spherical shapes) on a 400 mesh Cu grid stained with an aqueous solution containing 2% uranyl acetate. (b) Size distribution of **CD-$(HEG_7$-$PEG_9)_8$** calculated from TEM image displays a range of singular star polymers and their corresponding aggregates. (c) Number (%) DLS plots of **CD-$(HEG_7$-$PEG_9)_8$** demonstrating concentration-dependent aggregation in solution.

Having established the synthesis, structure, and physical properties of each DBASC, their ability to function as a drug delivery vehicle was evaluated next. The larger γ-CD macrocycle was chosen over β-CD because its bigger cavity allows for stronger binding of hydrophobic drugs, such as DOX·HCl, which is sparingly soluble in DMSO:aqueous buffer solutions. To support this claim, a titration was carried out and monitored by ^{1}H NMR, where DOX·HCl was titrated in aliquots of 0.1 equiv. into a 1 mM solution containing β-CD until two full equiv. were added. The same experiment was performed for γ-CD (data not shown), and the change in diagnostic proton

resonances associated with each CD host was plotted to determine the corresponding affinity constants (K_a). As expected, β-CD exhibited a binding affinity for DOX·HCl that was an order of magnitude lower than that obtained for the larger native γ-CD macrocycle (K_a = 10^2 versus 10^3 M^{-1}, respectively). Another set of titrations was also done with native γ-CD and **CD-(HEG$_7$-PEG$_9$)$_8$**, except instead of monitoring each by NMR, UV-Vis absorption spectroscopy was used instead (Fig. 12a-b). Similarly, the K_a values were calculated by plotting the change in absorbance at specific wavelengths as more guest (drug) was added to each host solution in concentrated aliquots. For both γ-CD and the DBASC, the binding affinity was found to be comparable (both 10^3 M^{-1}). However, we did observe two inflection points (at 1.0 and 2.5 equiv.) in the titration data (Fig. 12b) for the star polymer. We attribute this to the 1:1 binding by the γ-CD core, followed by residual binding by the star polymer's bulky diblock bottlebrush arms.

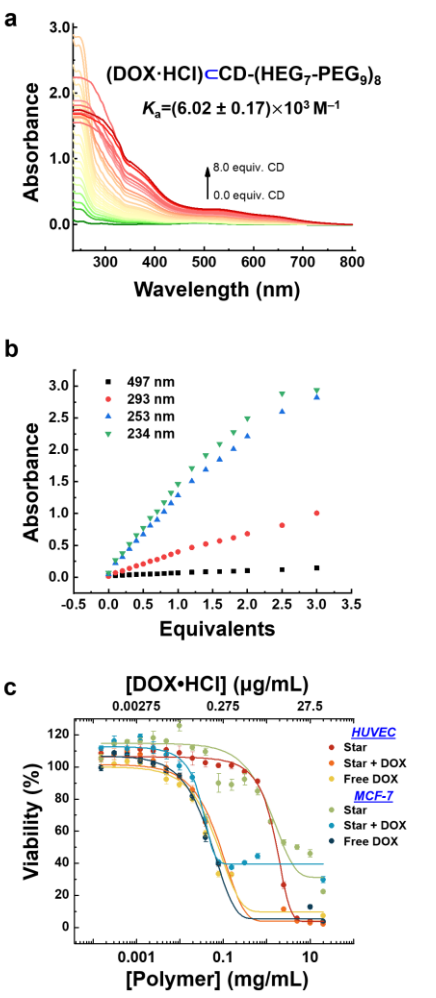

Figure 12. (a) Host-guest binding affinity titration monitored by UV-Vis absorbance spectroscopy as an increasing number of equiv. of DOX·HCl was added to a 1 mM aqueous solution containing DBASC. The binding affinity (K_a) was calculated by plotting the change in absorbance as a function of increasing concentrations of the guest (drug), where the data was entered and fitted using the resource supramolecular.org. (b) Change in absorbance (from Fig. 12a) plotted against number of equiv. of DOX·HCl added. (c) Cell viability plots for DBASC both empty and loaded with DOX·HCl, as well as with only free DOX·HCl, against a healthy HUVEC line and a breast cancer cell line (MCF-7).

To confirm the low toxicity of the DBASCs, a stock solution of **CD-(HEG$_7$-PEG$_9$)$_8$** (20 mg/mL) was diluted with media multiple times and incubated for 48 h with healthy human umbilical vein endothelial cells (HUVECs) in a 96-well plate (~5,000 cells/well). This experiment was also performed for the same DBASC loaded with DOX·HCl, as well as just for a solution containing free DOX·HCl. The results (Fig. 11b) of this viability assessment showed IC_{50} values of 1.64 mg/mL for empty DBASC and 0.08 mg/mL when loaded with one equiv. of the anticancer drug. The increased toxicity for the latter is expected considering DOX·HCl is an incredibly toxic drug. Comparing the DOX-loaded DBASC to free DOX·HCl, a higher concentration of the drug is needed to reach the IC_{50} value of HUVECs when bound by the DBASC versus the free drug (0.21 vs. 0.15 μg/mL of DOX). This lower toxicity is presumably due to the better solubility and slower release of the drug from the DBASC over time.

Lastly, the efficacy of the DBASC against MCF-7 was evaluated. Similar to the cytotoxicity studies, stock solutions of loaded and unloaded DBASC, as well as free DOX·HCl, were prepared and added to a 96-well plate containing the breast cancer cells (5,000 cells/well), followed by a 48 h incubation period. The live-dead cell viability assessment was carried out using a chemiluminescent assay and the results are plotted in Fig. 12c. Again, a higher concentration of the empty star polymer was needed to reach the IC_{50} value for MCF-7 cells in comparison to the DOX-loaded DBASC (0.87 vs. 0.03 mg/mL of star polymer). In terms of the DOX·HCl concentrations, only 0.09 μg/mL of drug bound by **CD-(HEG$_7$-PEG$_9$)$_8$** was needed to reach the IC_{50} value of MCF-7 cells, whereas 0.13 μg/mL of free

DOX·HCl was needed to reach the same level. This greater potency may also likely be due to the enhanced solubility of the anticancer drug when bound by the star polymer under the experimental conditions described here. The difference in toxicity may also potentially be attributed to enhanced cellular uptake when bound by the polymer, but we did not confirm this hypothesis. Nonetheless, the results from these cytotoxicity and anticancer efficacy studies demonstrate how lower drug loadings are required for treatment when carried by the non-toxic DBASC drug delivery vehicle.

Description of Use of Young Investigator Award Funds (see accompanying financial report)

The generous support of the Cancer Research Foundation in the form of a Young Investigator Award (YIA) has allowed my research group the time needed to develop two novel and next-generation nanoparticles for drug delivery. The majority of funds from the leftover first year and second year of the YIA went toward supporting graduate and postdoctoral researchers (~$30,237.36) who carried out the work in this progress report. The remaining funds (~$8,877) were used to purchase chemicals, solvents, and consumables, as well as pay for usage fees for instruments that were used to characterize the materials that were synthesized.

Future Goals in the Next Phase of Research

With the knowledge that we can form narrowly dispersed nanoparticles using non-covalent host-guest interactions as the mechanism for cross-linking the drug-loaded diblock copolymer, the next phase of this research is to assess the combination platform performance *in vivo*. This would be particularly useful for not only treating tumors, but also imaging them using the embedded Cy5.5 dye that is part of the polymer backbone. This proposed mouse study will include tail-vein injections of our dye-labeled nanoparticles will be carried out in female BALB/c mice in statistically relevant groups of 5 mice. In order to collect blood via cheek bleeds at the necessary time points, we would need 20 mice in total for the pharmacokinetic study to determine the half-life of the nanoparticles in the blood stream. These samples will be collected in a 96-well plate (with the necessary standards) and measured using a whole animal fluorimeter at the Molecular Imaging Center at WUSTL School of Medicine. Additionally, we will need to evaluate biodistribution to see which organ (kidney or liver) is predominantly responsible for clearing the non-covalently crosslinked nanoparticles. This work will be carried out on the medical school campus and we would be in direct consultation with Professor of Medicine and Director of the MIC, Dr. Samuel Achilefu and his team.

Once we have established the maximum tolerable doses, pharmacokinetics, and biodistribution, we will then assess the nanoparticles ability to administer different combinations of drugs in female NCr nude mice that have subcutaneous xenograft tumors seeded from OVCAR-3 and PANC-1 cancer cells. We will investigate the FOLFIRINOX combination of drugs, as well as other clinically relevant drug combinations and we will monitor the health of the mice, as well as the reduction in volume of their tumors. This data will be reported in two plots, a Kaplan Meier survival curve, and a tumor volume reduction versus time plot.

In all experiments involving live animals, we will follow the IACUC animal protocol at WUSTL for my group, and we will always try to minimize pain and stress for the mice that are the subjects of this investigation. The only time death will be an endpoint is if we need to sacrifice the mouse to excise its organs and image them *ex vivo*, or we need to get a pathology report on the condition of the mice organs. With my extensive experience performing this type of mouse model, I will be able to train and monitor the researchers in my group to make sure these studies are carried out in the most humane way possible.

Conclusions and Summary

Ultimately, the findings from the proposed research will open up a new universal strategy for drug delivery, where precise functional monomers are utilized to bind reversibly an assortment of drug cocktails that are frequently used to treat diseases, but which are incredibly toxic in their free drug forms. From a chemical perspective, this work will reveal a blueprint for how to design and synthesize next-generation functional polymers that can be used in a wide range of biomedical applications, and it will illustrate a new crosslinking strategy to make nanoparticles where the cross-linker is constantly undergoing dynamic exchange between CD cavities. This innovative platform brings to the forefront the notion of personalized medicine since any combination of small-molecule drugs can be encapsulated and delivered in concert.

References Cited

1 Editorial. Rationalizing combination therapies. *Nature Med*. **2017**, *23*, 1113.

2 National Cancer Institute (National Institutes of Health). https://www.cancer.gov/about-cancer/treatment/drugs/FOLFIRINOX (accessed July 17, 2017).

3 Peer, D.; Karp, J. M.; Hong, S.; Farokhzad, O. C.; Margalit, R.; Langer, R. Nanocarriers as an emerging platform for cancer therapy. *Nature Nanotech*. **2007**, *2*, 751–760.

4 Li, Z.; Barnes, J. C.; Bosoy, A.; Stoddart, J. F.; Zink, J. I. Mesoporous Silica Nanoparticles in Biomedical Applications. *Chem. Soc. Rev.* **2012**, *41*, 2590–2605.

5 Lu, J.; Liong, M.; Zink, J. I. Tamanoi, F. Mesoporous Silica Nanoparticles as a Delivery System for Hydrophobic Anticancer Drugs. *Small* **2007**, *3*, 1341–1346.

6 Croy, S. R.; Kwon, G. S. Polymeric Micelles for Drug Delivery. *Curr. Pharm. Des*. **2006**, *12*, 4669–4684.

7 Larson, N.; Ghandehari, H. Polymeric conjugates for drug delivery. **2012**, *24*, 840–853.

8 Verduzco, R.; Li, X.; Pesek, S. L.; Stein, G. E. Structure, function, self-assembly, and applications of bottlebrush copolymers. **2015**, *44*, 2405–2420.

9 Rosebrugh, L. E.; Marx, V. M.; Keitz, B. K.; Grubbs, R. H. Synthesis of Highly Cis, Syndiotactic Polymers via Ring-Opening Metathesis Polymerization Using Ruthenium Metathesis Catalysts. *J. Am. Chem. Soc.* **2013**, *135*, 10032–10035.

10 Grubbs, R. H. *Handbook of Metathesis* (1st ed.) Weinheim: Wiley-VCH (**2003**).

11 Williams, F. M. Clinical significance of esterases in man. *Clin. Pharmacokinet.* **1985**, *10*, 392–403.

12 Liu, Z.; Nalluri, K. M.; Stoddart, J. F. Surveying macrocyclic chemistry: from flexible crown ethers to rigid cyclophanes. *Chem. Soc. Rev*. **2017**, *46*, 2459–2478.

13 Irie, T.; Uekama, K. Pharmaceutical Applications of Cyclodextrins. III. Toxicological Issues and Safety Evaluation. *J. Pharm. Sci*. **1997**, *86*, 147–162.

14 Morohashi, N.; Narumi, F.; Iki, N.; Hattori, T.; Miyano, S. Thiacalixarenes. *Chem. Rev*. **2006**, *106*, 5291–5316.

15 Morones-Ramirez; J. R.; Winkler, J. A.; Spina, C. S.; Collins, J. J. Silver Enhances Antibiotic Activity Against Gram-Negative Bacteria. *Sci. Trans. Med*. **2013**, *5*, 190ra81.

16 deRonde, B.; Tew, G. N. Development of Protein Mimics for Intracellular Delivery. *Biopolymers* **2015**, *104*, 265–280.

17 Walsh, D. J.; Lau, S. H.; Hyatt, M. G.; Guironnet, D. Kinetic Study of Living Ring-Opening Metathesis Polymerization with Third-Generation Grubbs Catalysts. *J. Am. Chem. Soc*. **2017**, *139*, 13644–13647.

18 Szwarc, M. Living polymers. Their discovery, characterization, and properties. *J. Polym. Sci. Part A: Polym. Chem*. **1998**, *36*, ix-xv.

19 Bielawski, C. W.; Grubbs, R. H. Living ring-opening metathesis polymerization. *Prog. in Polym. Sci.* **2006**, *32*, 1–29.

20 Vougioukalakis, G. C.; Grubbs, R. H. Ruthenium-Based Heteocyclic Carbene-Coordinated Olefin Metathesis Catalysts. Chem. Rev. **2010**, *110*, 1746–1787.